

# *LncRNA-LINC00472* suppresses the malignant progression of non-small cell lung cancer via modulation of the *miRNA-1275/Homeobox A2* axis

Meichen Jiang<sup>1,D</sup>, Xiangli Ye<sup>2,C</sup>, Dongliang Shi<sup>1,B,C</sup>, Qili Lin<sup>1,C</sup>, Feijian Huang<sup>2,D</sup>, Yong Li<sup>2,A,E</sup>

<sup>1</sup> Department of Pathology, Fujian Medical University Union Hospital, Fuzhou, China

<sup>2</sup> Department of Respiration Medicine, Fujian Medical University Union Hospital, Fuzhou, China

A – research concept and design; B – collection and/or assembly of data; C – data analysis and interpretation;

D – writing the article; E – critical revision of the article; F – final approval of the article

Advances in Clinical and Experimental Medicine, ISSN 1899–5276 (print), ISSN 2451–2680 (online)

Adv Clin Exp Med. 2024;33(3):283–297

## Address for correspondence

Yong Li

E-mail: leo\_liyong9@163.com

## Funding sources

This study was sponsored by Fujian Provincial Health Technology Project (grant No. 2020GG8027), Natural Science Foundation of Fujian Province (grant No. 2021J01747) and Joint Funds for the Innovation of Science and Technology, Fujian province (grant No. 2021Y9043).

## Conflict of interest

None declared

Received on June 29, 2022

Reviewed on November 24, 2022

Accepted on June 16, 2023

Published online on September 4, 2023

## Cite as

Jiang M, Ye X, Shi D, Lin Q, Huang F, Li Y. *LncRNA-LINC00472* suppresses the malignant progression of non-small cell lung cancer via modulation of the *miRNA-1275/Homeobox A2* axis. *Adv Clin Exp Med*. 2024;33(3):283–297. doi:10.17219/acem/168431

## DOI

10.17219/acem/168431

## Copyright

Copyright by Author(s)

This is an article distributed under the terms of the Creative Commons Attribution 3.0 Unported (CC BY 3.0) (<https://creativecommons.org/licenses/by/3.0/>)

## Abstract

**Background.** Long non-coding RNAs (lncRNAs) are increasingly observed as regulatory factors for the initiation and progression of varying kinds of cancers. However, studies on lncRNAs in non-small cell lung cancer (NSCLC) progression are currently lacking.

**Objectives.** We intended to determine the role of lncRNA *LINC00472* and its downstream regulatory mechanism in NSCLC, thus providing novel ideas for targeted therapies for NSCLC.

**Materials and methods.** The target signaling axis comprising the lncRNA/microRNA/mRNA was identified through bioinformatics analysis. Subcellular localization of *LINC00472* was assessed with fluorescence in situ hybridization (FISH). Cellular function experiments were conducted to examine the proliferation, migration, invasion, and apoptosis of NSCLC cells, and dual-luciferase and RNA binding protein immunoprecipitation assays were performed to validate the binding relationship. Quantitative real-time polymerase chain reaction (qPCR) and western blot were utilized to assess the expression levels of the investigated gene and protein, respectively.

**Results.** The *LINC00472* expression was markedly decreased in NSCLC tissues and cells. The FISH, combined with nuclear–cytoplasm separation assay, demonstrated that *LINC00472* was mainly located in the cytoplasm. The overexpression of *LINC00472* restrained proliferation and metastasis of NSCLC in vitro. The *LINC00472* could target and repress *miR-1275* level, and overexpression of *LINC00472* reduced the *miR-1275*-dependent malignant cell phenotype in NSCLC. Further study revealed that *HOXA2* was a downstream target of *miR-1275* and was negatively modulated by *miR-1275*. Rescue assays exhibited that the overexpression of *miR-1275* or inhibition of *HOXA2* reversed the impact of *LINC00472* overexpression on the malignant progression of NSCLC cells. The *LINC00472* repressed the epithelial–mesenchymal transition (EMT) of NSCLC cells through *miR-1275/HOXA2*.

**Conclusions.** The *LINC00472* functioned as a competing endogenous RNA to modulate *HOXA2* level by sponging *miR-1275* in NSCLC. Simultaneously, the *LINC00472/miR-1275/HOXA2* axis may be a possible therapeutic target and biomarker for NSCLC.

**Key words:** NSCLC, *miR-1275*, malignant progression, *LINC00472*, *HOXA2*

## Background

Lung cancer (LC) reaches the highest mortality rates among cancers throughout the world,<sup>1</sup> and 85% of cases are categorized as non-small cell lung cancer (NSCLC).<sup>1,2</sup> Few NSCLC patients are diagnosed at an early stage,<sup>3</sup> and more than 60% of LC patients are already at an advanced stage or have tumor metastasis (stage III or IV) at the first diagnosis, precluding surgical resection. Until now, chemotherapy and radiotherapy have been the main treatment methods for this disease.<sup>4</sup> Despite progress in LC clinical diagnosis and therapy, neither new targeted therapy nor immunotherapy has been able to yield a desirable effect,<sup>4</sup> with the 5-year overall survival (OS) of less than 20%.<sup>5,6</sup> Therefore, elucidating the molecular mechanism underlying NSCLC progression and exposing potential diagnostic and treatment targets are essential.

Long non-coding RNAs (lncRNAs) have no or limited protein-coding potential.<sup>7</sup> They have been widely studied for their ability to sponge microRNA (miRNA) and regulate downstream gene expression, and lncRNA mutations or disorders play an important role in cancer.<sup>8</sup> The *LINC00472* is an intergenic lncRNA<sup>9</sup> located on chromosome 6q13, and its abnormal expression is implicated in many biological processes and tumor progression.<sup>10</sup> It is reported that *LINC00472* has an antitumor effect in breast cancer,<sup>11,12</sup> and is negatively correlated with the breast cancer tumor-node-metastasis (TNM) stage.<sup>13</sup> Moreover, the *LINC00472* level in epithelial ovarian cancer (EOC) is also related to TNM stage.<sup>14</sup> The *LINC00472* has been shown to repress proliferation and enhance apoptosis of colorectal cancer (CRC) cells by mediating the *miR-196a/PDCD4* axis.<sup>9</sup> In hepatocellular carcinoma (HCC), *LINC00472* can inhibit the malignant phenotype via regulating the *miR-93-5p/PDCD4* axis.<sup>15</sup> Although it has been reported that *LINC00472* has a potential regulatory role in LC<sup>16</sup> and NSCLC<sup>17,18</sup> and is a candidate biomarker for diagnosis and treatment, the role of *LINC00472* in NSCLC progression requires further investigation.

The miRNAs can modulate downstream targeted genes<sup>19</sup> through the complementary pairing of mRNA 3'-UTR ends at the post-transcriptional level. According to reports, *miR-21*,<sup>20</sup> *miR-1253*<sup>21</sup> and *miR-3607-3p*<sup>22</sup> participate in the progression of NSCLC through different cellular processes. The *miR-1275* is pivotal in different tumors, such as bladder cancer,<sup>23</sup> nasopharyngeal carcinoma (NPC)<sup>24</sup> and esophageal cancer.<sup>25</sup> In addition, *PGM5P4-AS1* can inhibit the malignant behavior of LC cells through sponging *miR-1275*.<sup>26</sup> However, investigations regarding *miR-1275* in NSCLC have been lacking.

*Homeobox A2* (*HOXA2*) belongs to the *HOX* family,<sup>27</sup> whose members are involved with multiple cancer types. For instance, *HOXB5* restrains NSCLC cell phenotype progression by inactivating the *Wnt/β-catenin* pathway,<sup>28</sup> and it also has an association with CRC,<sup>29</sup> NPC<sup>30</sup> and breast

cancer.<sup>31</sup> The *HOXA2* can play a regulatory role in the malignant progression of glioma cells, and its elevated expression reflects a poor prognosis for glioma patients.<sup>32</sup> Furthermore, *HOXA2* is a common hypermethylation marker gene in squamous cell carcinoma and is associated with its prognosis.<sup>33</sup> However, the molecular mechanism of *HOXA2* and its effects on NSCLC have not been thoroughly studied.

## Objectives

This study combined bioinformatics analysis as well as molecular and cell function experiments to explore the influence of the lncRNA-*LINC00472*/miR-1275/*HOXA2* axis on the malignant progression of NSCLC, providing a theoretical basis for finding novel targeted treatment method.

## Materials and methods

### Bioinformatics analysis

The NSCLC gene expression chips GSE44077 and GSE102286 were obtained through the Gene Expression Omnibus (GEO) database, where GSE44077 contains mRNA expression data (normal: n = 66, tumor: n = 55) and GSE102286 is composed of miRNA expression data (normal: n = 88, tumor: n = 91). The R package “limma”<sup>34</sup> was introduced for differential analysis, with  $|\log FC| > 1$  and p-value < 0.05 set as thresholds. Regulatory miRNAs downstream of *LINC00472* were predicted using the RNA22 database, and target genes downstream of *miR-1275* were predicted via TargetScan (<https://www.targetscan.org>), miRSearch (<https://www.mirbase.org/search.shtml>) and mirDIP (<http://ophid.utoronto.ca/mirDIP>).

### Cell culture

Cell line information is shown in Table 1. The normal human lung epithelial cell line BEAS-2B and NSCLC cell lines NCI-H1975, NCI-H157, NCI-H358, and NCI-H1299

**Table 1.** Cell lines used in the assay (all obtained from Cobioer, Nanjing, China)

Cell line	Cell type	Product code
BEAS-2B	human lung (bronchus) epithelial cell line	CBP60577
NCI-H1975	human adenocarcinoma cell line	CBP60121
NCI-H157	human squamous cell carcinoma cell line	CBP60952
NCI-H358	human NSCLC cell line	CBP60136
NCI-H1299	human NSCLC cell line	CBP60053
293T	human embryonic kidney cell	CBP60440

NSCLC – non-small cell lung cancer.

were maintained in Roswell Park Memorial Institute-1640 (RPMI-1640) complete medium (cat. No. MFC00217820; Sigma-Aldrich, St. Louis, USA). Human embryonic kidney cell line 293T was maintained in Dulbecco's modified Eagle's medium (DMEM, cat. No. M3942; Sigma-Aldrich). All media contained an additional 10% fetal bovine serum (FBS; cat. No. 10099141; Gibco, Grand Island, USA), 100 U/mL penicillin and 100 µg/mL streptomycin sulfate (cat. No. 30-002-CI; Corning Inc., Corning, USA), and cultures were maintained at 37°C with 5% CO<sub>2</sub>. After sterilizing the purchased cell lines with 75% alcohol, we observed cell shape, adhesion and density under an inverted microscope (model CKX53; Olympus Corp., Tokyo, Japan). Then, we put cells in a 37°C and 5% CO<sub>2</sub> cell incubator (model BB150; Thermo Fisher Scientific, Waltham, USA) for 2–3 h to stabilize them before further experiments.

## Cell transfection

The sequence of *LINC00472* (full-length) was cloned using the SMARTer™ RACE cDNA kit (cat. No. 634858/59; Takara, Kusatsu, Japan). The *LINC00472* overexpression vector (oe-*LINC00472*) and empty pcDNA3.1 vector (cat. No. V79020, oe-NC) were obtained from Thermo Fisher Scientific, and following lentiviral transduction, infected cell lines NCI-H358 and NCI-H1299 were treated with 1 mg/mL puromycin to generate stably transfected cell lines. The *miR-1275* mimic (miR-mimic) and blank control (miR-NC) were obtained from RiboBio Co., Ltd. (Guangzhou, China), and *HOXA2* silencing plasmids (si-*HOXA2*) and pLenti vectors (si-NC) were purchased from Vigene Biosciences (Rockville, USA). Lipofectamine™ 3000 (cat. No. L3000015; Invitrogen, Waltham, USA) was employed for transfection. Cells were harvested 48 h after transfection, with the transfection efficiency being assessed using quantitative real-time polymerase chain reaction (qPCR).

## qPCR

The total RNA of each cell line (BEAS-2B, NCI-H1975, NCI-H157, NCI-H358, and NCI-H1299) was extracted and quantified. Total RNA was extracted using TRIzol™ reagent (cat. No. 10296010; Thermo Fisher Scientific), and the RNA concentration was assessed using a NanoDrop™ 2000 (Thermo Fisher Scientific). The miScript II RT kit (cat. No. 18064071; Qiagen, Hilden, Germany) was used to synthesize cDNA by reverse transcription from miRNA, miScript SYBR Green PCR Kit (cat. No. 4309155; Qiagen) was used for detection, and U6 was utilized as the internal reference. Using PrimeScript RT Master Mix (cat. No. RR036Q; Takara), lncRNA and mRNA were reverse transcribed into cDNA. Additionally, SYBR® Premix Ex Taq™ II (cat. No. RR820A; Takara) was utilized for assessment, and GAPDH was the endogenous control. All qPCR tests were performed on an Applied Biosystems® 7500 Real-Time PCR Systems (cat. No. 4362143; Thermo

**Table 2.** Primer sequence used in quantitative real-time polymerase chain reaction (qPCR)

Gene	Sequence	
<i>LINC00472</i>	forward	5'-GATGGCAGCTGTCTCTCTCC-3'
	reverse	5'-GGGCCTCTCTGACCGTATCT-3'
<i>GAPDH</i>	forward	5'-GGGCCAAAAGGGTCATCATC-3'
	reverse	5'-ATGACCTTGCCACAGCCTT-3'
<i>miR-1275</i>	forward	5'-TGGGGGAGAGGCTGTC-3'
	reverse	5'-GAACATGTCTGCGTATCTC-3'
<i>U6</i>	forward	5'-CTCGCTTCGGCAGCACAT-3'
	reverse	5'-TTTTCGTGTCATCTTTCGCG-3'
<i>HOXA2</i>	forward	5'-GGGTATTYGGYGGTTGTAGG-3'
	reverse	5'-AATACCTAACATCTTTCCCTATC-3'

Fisher Scientific). Primer information is available in Table 2. The  $2^{-\Delta\Delta C_t}$  method was applied for relative expression calculations, and the experiment was performed in triplicate.

## Fluorescence in situ hybridization and subcellular separation

The lncRNA *LINC00472* fluorescence in situ hybridization (FISH) probe was labeled with 5-carboxyfluorescein and synthesized by Biolite Corp (cat. No. 76823-03-5; Xi'an, China). Following protease K digestion, the tissue was denatured with formamide and hybridized overnight with the *LINC00472* probe at 42°C, followed by staining with 300 µL 4,6-diamino-2-phenyl indole (DAPI; cat. No. 28718-90-3; Solarbio, China). Samples were analyzed with the use of laser scanning confocal microscope (model LSM700; Carl Zeiss, Oberkochen, Germany), and the nucleus and cytoplasm of NCI-H358 and NCI-H1299 cells were separated using PARIS Kit (cat. No. AM1921; Thermo Fisher Scientific).

## Cell Counting Kit-8 assay

Cells were seeded into 96-well plates ( $2 \times 10^4$  cells/well) under routine conditions and grown at 70% confluence. After 0, 24, 48, and 72 h, 10-microliter Cell Counting Kit-8 (CCK-8) solution (cat. No. CK04; Dojindo Laboratories, Kumamoto, Japan) was administered to each well, followed by a 2-hour incubation. The optical density was assessed at 450 nm using a microplate reader (Multiskan MK3; Thermo Fisher Scientific), and the experiment was performed 3 times.

## Transwell assay

### Cell invasion

Cells ( $1 \times 10^4$  cells/well) were added to the upper insert of 24-well transwell chambers (8 µm in diameter; cat. No. 3428; Corning Inc.) coated with Matrigel. The lower chamber was filled with RPMI-1640 complete medium (cat.

No. R4130; Sigma-Aldrich) and 10% FBS (cat. No. 10099141; Gibco). Following 36 h of incubation at 37°C, we utilized a wet applicator to remove cells that did not pass the membrane, and cells on the lower surface underwent fixation with 4% paraformaldehyde and staining with 0.5% crystal violet. After staining, cells were imaged using an inverted microscope (model CKX53; Olympus Corp.).

### Cell migration

After 24 h of starvation, log phase cells were digested, centrifuged and resuspended the next day to a concentration of  $2 \times 10^4$  cells/mL. A total of 0.2 mL of the cell suspension was seeded to the upper chamber, with the lower chamber being filled with 700  $\mu$ L of precooled RPMI-1640 complete medium and 10% FBS. After maintaining cells in routine conditions for 36 h, we removed cells that did not migrate, and fixed the migrated cells with methanol for 30 min. Cells were stained with 0.5% crystal violet for 20 min, washed, inverted, and dried naturally, followed by imaging under an inverted microscope (model CKX53; Olympus Corp.). We selected 5 visual fields to count the visible cells.

### Annexin V/propidium iodide double staining assay

Trypsin without ethylenediamine tetra-acetic acid (EDTA) was used to treat log phase cells, which were centrifuged, and the supernatant was discarded. Cells were rinsed twice with phosphate-buffered saline (PBS), and then resuspended with 500  $\mu$ L of precooled  $1 \times$  binding buffer until the concentration reached  $1 \times 10^6$  cells/mL. A total of 100  $\mu$ L of cell suspension was added with 5  $\mu$ L of Annexin-V-FITC (cat. No. C1062S; Beyotime, Shanghai, China) at room temperature for 15 min in the dark. After that, 2.5  $\mu$ L of propidium iodide (PI) staining solution (cat. No. 25535-16-4; MedChemExpress, Belleville, USA) was added 5 min before the analysis using a flow cytometer (cat. No. A29003; Thermo Fisher Scientific). FlowJo v. 10 software (FlowJo LLC, Ashland, USA) was used to analyze apoptosis. The experiment was repeated 3 times.

### Dual-luciferase reporter gene analysis

The pmirGLO luciferase reporter vectors (cat. No. E1330; Promega, Madison, USA) inserted with wild-type (WT) and mutant (MUT) *LINC00472* or *HOXA2* 3'UTR were built, respectively. The 293T cells were maintained in 24-well plates and transfected based on the co-transfection groups (miR-mimic + *LINC00472*-WT or *LINC00472*-MUT; miR-NC + *LINC00472*-WT or *LINC00472*-MUT; miR-mimic + *HOXA2*-WT or *HOXA2*-MUT; miR-NC + *HOXA2*-WT or *HOXA2*-MUT). Then, 48 h after transfection, luciferase activity was measured with a dual-luciferase reporter system (cat. No. E1910; Promega).

### RNA binding protein radioimmunoprecipitation assay

Magna RNA immunoprecipitation kit (cat. No. 17-704; Millipore, Burlington, USA) was used according to the manufacturer's instructions. After being maintained in radioimmunoprecipitation (RIP) buffer with magnetic beads, cell lysates were combined with rabbit anti-Ago2 antibody. Input or rabbit immunoglobulin G (IgG) was utilized as the negative control (NC). Protease K (cat. No. HY-108717; MCE) was utilized to purify and immunoprecipitate the RNA of both the samples and the inputs. Next, RNA was isolated for qPCR analysis. Antibody information is displayed in Table 3.

**Table 3.** Antibody information used in the assay (all antibodies purchased from Abcam, Cambridge, UK)

Antibody	Application	Dilution ratio	Product code	Specificity
Anti-HOXA2	western blot	1:2000	ab229960	rabbit
Anti-E-cadherin		1:10,000	ab40772	rabbit
Anti-N-cadherin		1:10,000	ab76011	rabbit
Anti-MMP2		1:5000	ab92536	rabbit
Anti-MMP9		1:10,000	ab76003	rabbit
Anti-Bax		1:5000	ab32503	rabbit
Anti-Bcl-2		1:1000	ab32124	rabbit
Anti-GAPDH		1:10,000	ab181602	rabbit
Anti-Argonaute-2	RIP	–	ab32381	rabbit
IgG		–	ab172730	rabbit
Anti-HOXA2	IHC	1:2000	ab229960	rabbit
Anti-Ki67		1:500	ab15580	rabbit
IgG		1:1000	ab6721	goat anti-rabbit

RIP – RNA immunoprecipitation; IHC – immunohistochemistry.

### Western blot assay

The extraction of total proteins from cells was performed using RIP assay (RIPA; cat. No. P0013B; Beyotime), and protein concentration was assessed with a bicinchoninic acid (BCA) protein assay kit (cat. No. P0011; Beyotime). After denaturation at a high temperature, proteins were isolated using sodium dodecyl sulfate–polyacrylamide gel electrophoresis (SDS-PAGE), followed by a transfer to polyvinylidene fluoride (cat. No. 24937-79-9; Millipore) membranes. Membranes were blocked with 5% bovine serum albumin (BSA) at room temperature for 2 h, and probed with primary antibodies overnight at 4°C. Relevant information about primary antibodies is shown in Table 3. Membranes were incubated with the secondary antibody goat anti-rabbit IgG H&L (HRP) (cat. No. ab205718; Abcam, Cambridge, UK) for 2 h at room temperature. The protein blots on the membrane were detected using an enhanced chemiluminescence kit (ECL; cat. No. P0018S; Beyotime).



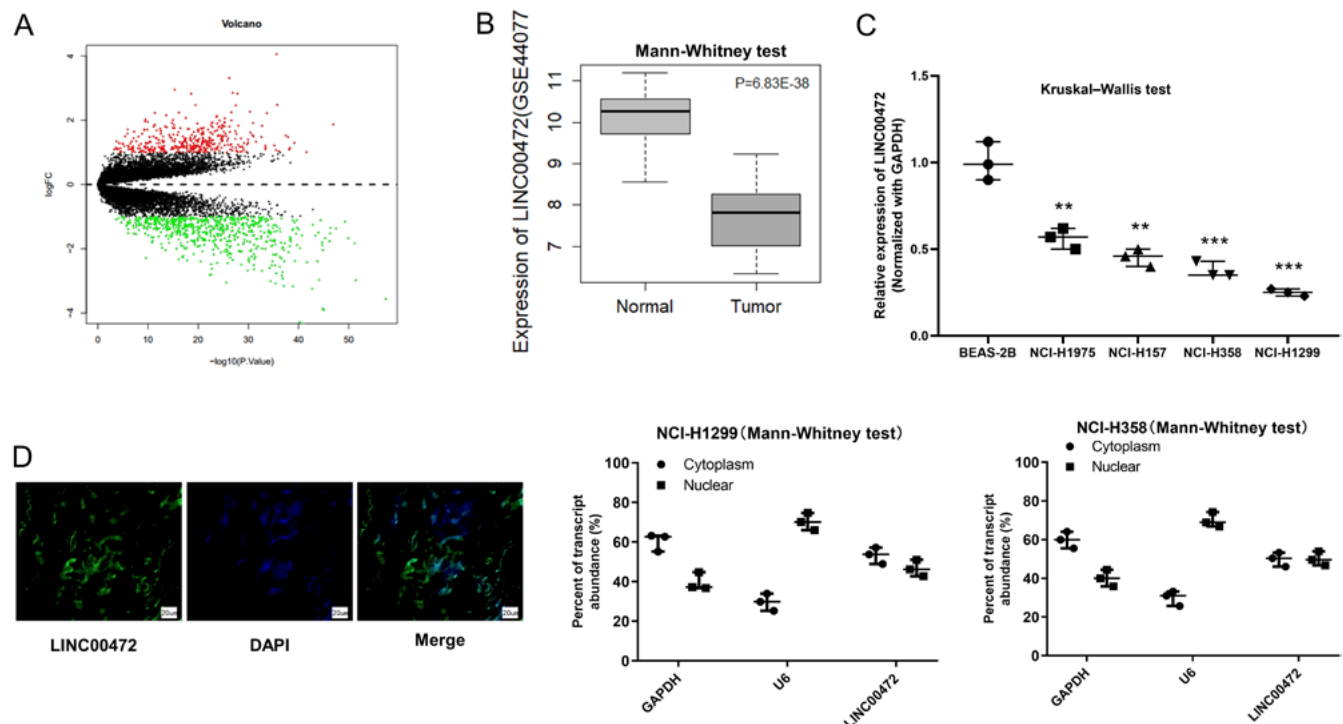


**Fig. 1.** *LINC00472* is downregulated in non-small cell lung cancer (NSCLC) and predominantly located in the cytoplasm. A. Volcano map of differential genes in NSCLC gene expression chip GSE44077. X-axis represents the  $\log_{10}$  p-value, while Y-axis represents the  $\log_2 FC$  value; the red points represent significantly upregulated genes in the tumor, the green points represent markedly downregulated genes in the tumor, and the black points represent genes with no significant difference; B. *LINC00472* level in normal (left) and tumor (right) groups in GSE44077. X-axis: sample type, Y-axis: lncRNA expression value (Mann-Whitney U test (M-W)); C. *LINC00472* level in NSCLC cells (NCI-H1975, NCI-H157, NCI-H358, and NCI-H1299) and normal cells (BEAS-2B) was assayed using quantitative real-time polymerase chain reaction (qPCR) (Kruskal-Wallis test); D. Fluorescence in situ hybridization (FISH) (400 $\times$ ) was conducted to verify location of *LINC00472* in NSCLC tissues. After the nuclei and cytoplasm of NCI-H1299 and NCI-H358 cells were separated, the expression of *GAPDH* (cytoplasmic marker), *U6* (nuclear marker) and *LINC00472* was assessed (M-W; \*\* $p < 0.01$ ; \*\*\* $p < 0.001$ ). The horizontal lines represent the medians

## Statistical analyses

GraphPad Prism v. 8.0.2 (GraphPad Software, San Diego, USA) was employed for data processing, and all experiments were performed in triplicate. All experimental data are shown as raw data, and due to limited sample size, all data were assessed with nonparametric tests. The Mann-Whitney U test (M-W) was used for a comparison between 2 groups, and the Kruskal-Wallis test was used for a comparison of 3 or more groups, followed by Dunn's post hoc test. The medians with 95% confidence interval (95% CI) whiskers are presented in results.<sup>35</sup> The reference sample shown in Fig. 1A and Fig. 1B is the normal group, the reference sample shown in Fig. 1C is the BEAS-2B cell line, the reference sample presented in Fig. 2 is the oe-NC group, and the reference sample displayed in Fig. 3 is the miR-NC group. In Fig. 4, the oe-NC+miR-NC group is the reference sample for the oe-NC+miR-mimic group, while the oe-NC+miR-mimic group is the reference sample for the oe-*LINC00472*+miR-mimic group. The reference sample in Fig. 5B is the normal group. The reference sample in Fig. 5D-F is the miR-NC group. Fig. 5A is the interaction of sets from 4 databases that down-regulate miRAN without reference groups, and Fig. 5C is sequence information without reference groups In Fig. 5G,H and

Fig. 6, the NC group is the reference sample for the oe-*LINC00472* group, and the oe-*LINC00472* group is the reference sample for the oe-*LINC00472*+miR-mimic group and oe-*LINC00472*+si-*HOXA* group. All experiments were performed in triplicate. Statistical significance was determined at  $p < 0.05$ , while  $p < 0.010$  suggested a significant difference and  $p < 0.001$  indicated an extremely significant difference.

## Results

### *LINC00472* is downregulated and mainly located in the cytoplasm in NSCLC

The NSCLC gene expression chip GSE44077 was obtained from the GEO database, with differential analysis finding 1029 differentially expressed genes (Fig. 1A). The *LINC00472* was dramatically underexpressed in NSCLC tissues (Fig. 1B,  $p < 0.001$ , M-W), suggesting that *LINC00472* may be pivotal in NSCLC progression. In addition, the *LINC00472* level in BEAS-2B, NCI-H1975, NCI-H157, NCI-H358, and NCI-H1299 cells was assessed using qPCR. Compared with BEAS-2B, *LINC00472* expression was lower in 4 NSCLC cell lines,

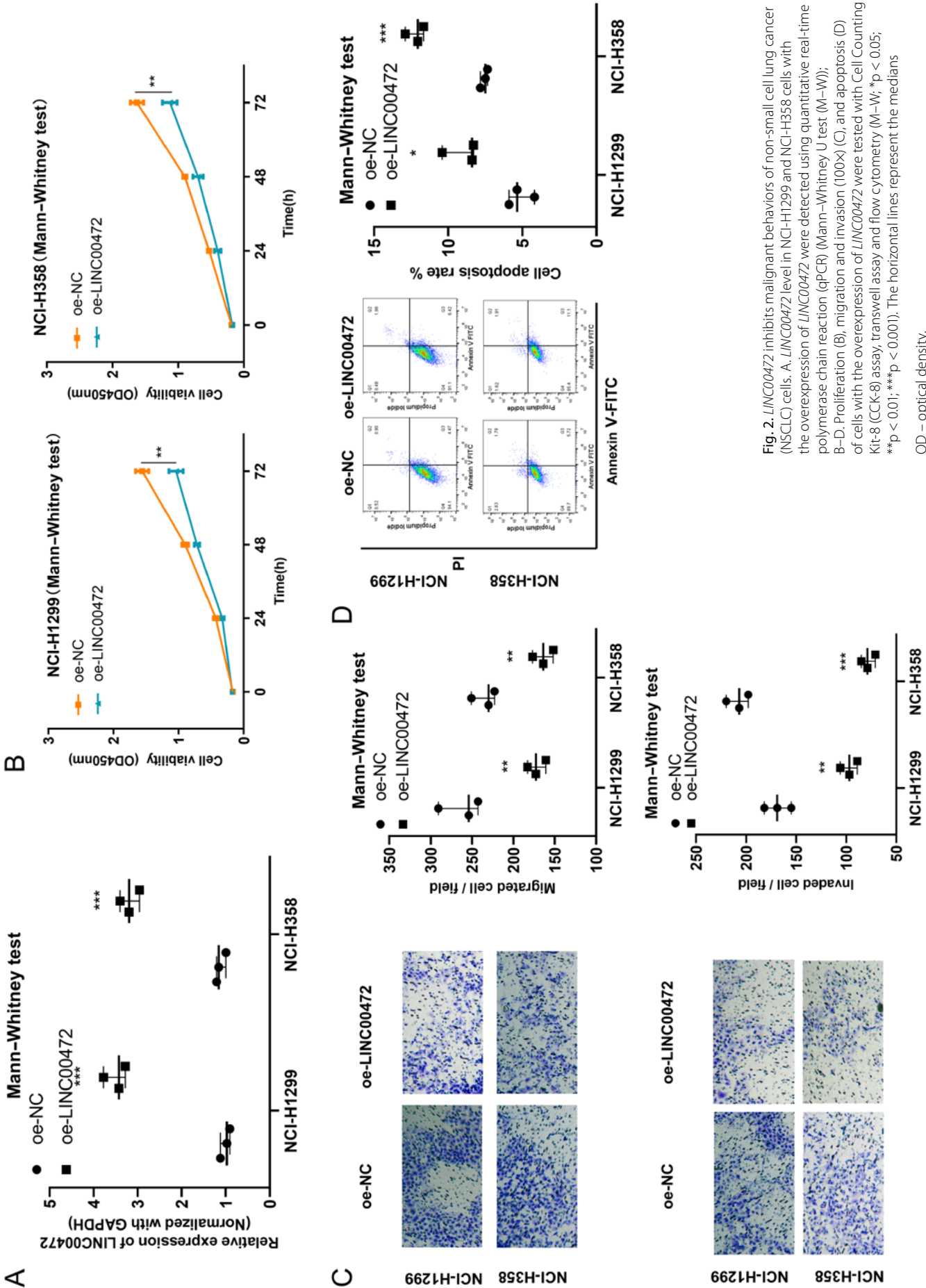
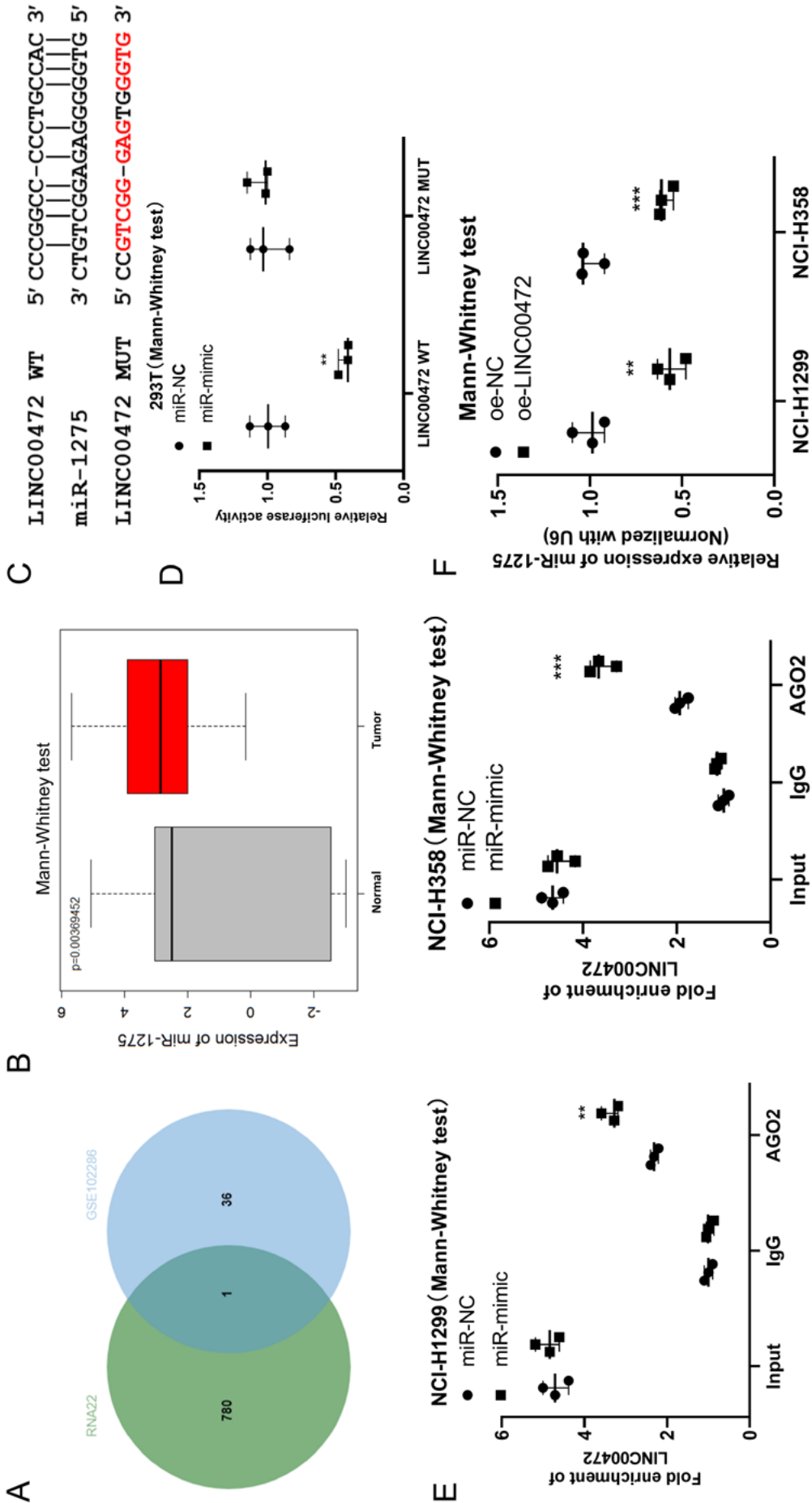


Fig. 2. LINC00472 inhibits malignant behaviors of non-small cell lung cancer (NSCLC) cells. A. LINC00472 level in NCI-H1299 and NCI-H358 cells with the overexpression of LINC00472 were detected using quantitative real-time polymerase chain reaction (qPCR) (Mann-Whitney U test (M-W)); B-D. Proliferation (B), migration and invasion (100×) (C), and apoptosis (D) of cells with the overexpression of LINC00472 were tested with Cell Counting Kit-8 (CCK-8) assay, transwell assay and flow cytometry (M-W; \*p < 0.05; \*\*p < 0.01; \*\*\*p < 0.001). The horizontal lines represent the medians OD – optical density.



**Fig. 3.** *LINC00472* targets to inhibit *miR-1275* level in NSCLC cells. **A.** Identification of the downstream miRNA of *LINC00472*. The left side is the prediction result of the RNA22 database, the right side is the differential analysis result of the GSE102286 chip, and the overlapped part is the intersection of the 2 groups of data; **B.** *miR-1275* level in normal (grey) and tumor (red) groups in GSE102286 (Mann-Whitney U test (M-W)); **C.** Binding sites between *LINC00472* and *miR-1275* were predicted; **D.** The relationship between *LINC00472* and *miR-1275* was confirmed using dual-luciferase assay (M-W); **E.** RNA immunoprecipitation (RIP) was used to validate the relationship between *LINC00472* and *miR-1275* in NCI-H1299 and NCI-H358 cells (M-W); **F.** *miR-1275* level in cells after *LINC00472* was overexpressed (M-W; \*\*,  $p < 0.01$ ; \*\*\*,  $p < 0.001$ ). The horizontal lines represent the medians

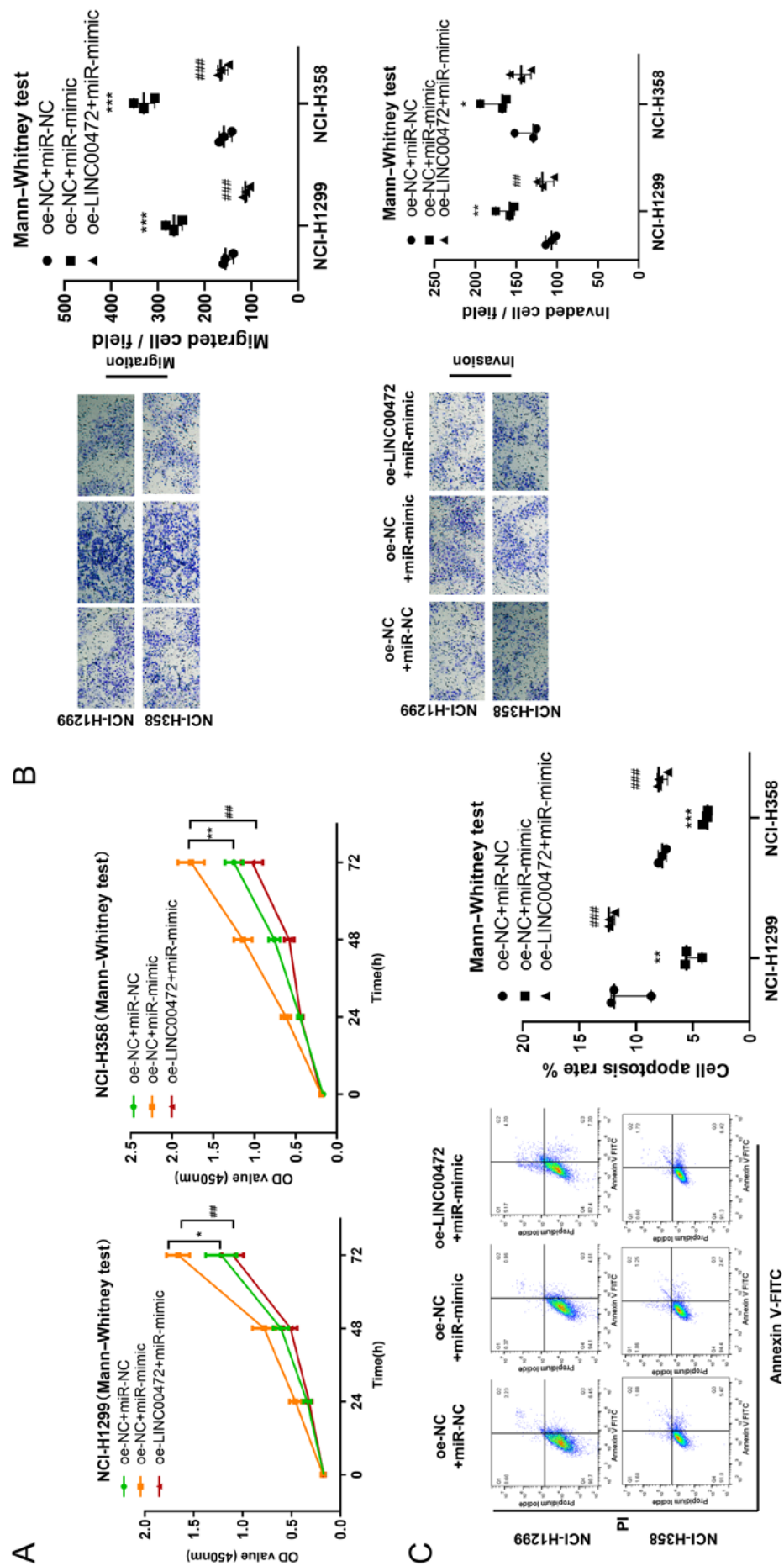
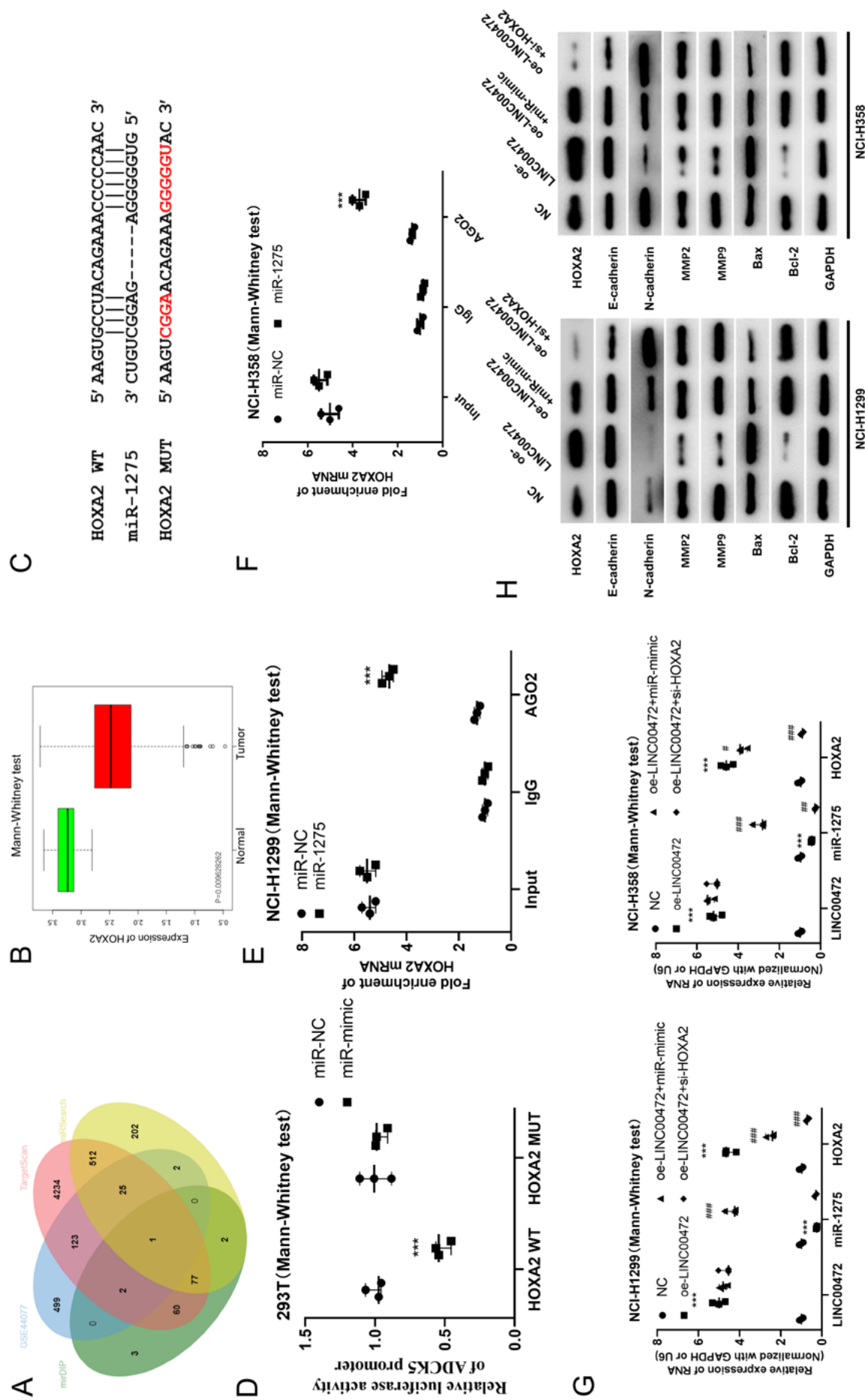


Fig. 4. LINC00472 reverses the impact of miR-1275 on the malignant phenotype of non-small cell lung cancer (NSCLC) cells. A–C. Proliferation (A), migration and invasion (100X) (B), and apoptosis (C) of NCI-H1299 and NCI-H358 cells were tested with Cell Counting Kit-8 (CCK-8) assay, transwell assay and flow cytometry in each group (Mann–Whitney U test). The horizontal lines represent the medians

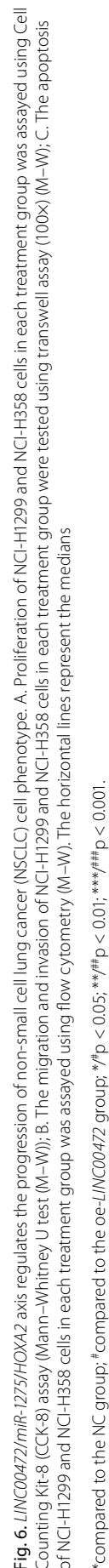
OD – optical density; \*compared to the NC group; # compared to the oe-NC+miR-mimic group; \* $p < 0.05$ ; \*\* $p < 0.01$ ; \*\*\* $p < 0.001$ .





**Fig. 5.** *LINC00472* promotes *HOXA2* expression level and affects epithelial–mesenchymal transition (EMT), metastasis and apoptosis-related protein levels via inhibiting *miR-1275*. **A.** Identification of the downstream targeted gene of *miR-1275*. Four ellipses in the picture respectively represent differentially downregulated genes in GSE44077, prediction results of TargetScan database, miRIP and miRSearch databases, and the overlapped part represents the intersection of data in 4 groups. **B.** Boxplot of *HOXA2* gene level in normal (green) and tumor (red) groups in GSE44077 (Mann–Whitney U test (M–W)). **C.** Predictive binding sites between *miR-1275* and *HOXA2*; **D.** The targeted relationship confirmed with dual luciferase analysis (M–W); **E,F.** The targeted relationship between *miR-1275* and *HOXA2* in NCI-H1299 and NCI-H358 cell lines were determined using RNA immunoprecipitation (RIP) assay (M–W); **G.** mRNA expression levels of *LINC00472*, *miR-1275* and *HOXA2* in each group were tested with the use of quantitative real-time polymerase chain reaction (qPCR) (M–W); **H.** The protein expression of *HOXA2*, *E-cadherin*, *N-cadherin*, *MMP2*, *MMP9*, *Bax*, and *Bcl-2* proteins as determined using western blot. The horizontal lines represent the medians

\*compared to the NC group; #compared to the oe-*LINC00472* group; \**p* < 0.05; \*\**p* < 0.01; \*\*\**p* < 0.001; \*\*\*/###*p* < 0.001.



especially in NCI-H358 and NCI-H1299 (NCI-H1975 compared to BEAS-2B,  $p < 0.010$ ; NCI-H157 compared to BEAS-2B,  $p < 0.010$ ; NCI-H358 compared to BEAS-2B,  $p < 0.001$ ; NCI-H1299 compared to BEAS-2B,  $p < 0.001$ ; Kruskal–Wallis test with Dunn's post hoc test) (Fig. 1C). Therefore, in vitro experiments were conducted on NCI-H1299 and NCI-H358 cell lines.

Previous studies have highlighted that *LINC00472* could play a modulatory role via the expression of ceRNA.<sup>9,18</sup> The FISH and nuclear–cytoplasm separation assays verified that *LINC00472* mainly existed in the cytoplasm (Fig. 1D,  $p > 0.050$ , M–W), and hence, *LINC00472*, as a ceRNA, may regulate the levels of downstream targeted genes by binding to miRNA.

### ***LINC00472* represses malignant behaviors of NSCLC cells**

Based on the *LINC00472* level in tumor tissues and cells, we hypothesized that *LINC00472* had a negative correlation with NSCLC progression. Therefore, we speculated that the overexpression of *LINC00472* in NSCLC cells could affect cancer progression. First, we overexpressed *LINC00472* in NCI-H1299 and NCI-H358 cells, and detected its transfection efficiency using qPCR (NCI-H1299,  $p < 0.001$ ; NCI-H358,  $p < 0.001$ ; M–W). Thus, the transfected cell lines could be utilized for subsequent experiments (Fig. 2A).

Then, we examined the impact of the overexpression of *LINC00472* on cell proliferation. The CCK-8 assay disclosed that the overexpression of *LINC00472* noticeably reduced the proliferative ability of both cell lines (NCI-H1299,  $p < 0.010$ ; NCI-H358,  $p < 0.010$ ; M–W) (Fig. 2B). Next, we assessed the influence of *LINC00472* on NSCLC cell migration and invasion, and we demonstrated notable repression (migration: NCI-H1299,  $p < 0.010$ ; NCI-H358,  $p < 0.010$ ; invasion: NCI-H1299,  $p < 0.010$ ; NCI-H358,  $p < 0.001$ ; M–W) (Fig. 2C). In addition, the cell apoptosis assay highlighted that the overexpression of *LINC00472* significantly upregulated cell apoptosis (NCI-H1299,  $p < 0.050$ ; NCI-H358,  $p < 0.001$ ; M–W) (Fig. 2D). Thus, *LINC00472* could be characterized as a tumor repressor by restraining malignant NSCLC cell behaviors.

### ***LINC00472* sponges *miR-1275* in NSCLC cells**

Modulatory miRNA downstream of *LINC00472* was predicted using the RNA22 database. Concurrently, significantly upregulated miRNAs were obtained through differential analysis of NSCLC miRNA chip GSE102286. Through the intersection of the predicted results and the differentially upregulated miRNAs (Fig. 3A), we identified *miR-1275* to be highly expressed in NSCLC tissues (Fig. 3B,  $p < 0.010$ , M–W).

To further understand the molecular regulatory mechanism of *LINC00472* and *miR-1275*, their binding sites were predicted through a bioinformatics analysis (Fig. 3C), which was then verified with a dual-luciferase analysis. The overexpression of *miR-1275* could inhibit luciferase activity of *LINC00472*-WT (293T,  $p < 0.010$ , M–W) but did not influence *LINC00472*-MUT (293T,  $p > 0.050$ , M–W), highlighting their targeted relationship (Fig. 3D). Subsequently, we conducted a RIP assay, which confirmed the targeted relationship (AGO2: NCI-H1299,  $p < 0.01$ ; NCI-H358,  $p < 0.001$ ; M–W) (Fig. 3E). Next, we tested *miR-1275* expression in NCI-H358 and NCI-H1299 cells after overexpressing *LINC00472*. The results demonstrated that the *miR-1275* level was significantly reduced after *LINC00472* overexpression (NCI-H1299,  $p < 0.010$ ; NCI-H358,  $p < 0.001$ ; M–W) (Fig. 3F). The above results unveiled a direct interaction between *LINC00472* and *miR-1275* in NSCLC, and *LINC00472* was able to be a molecular sponge of *miR-1275*.

### ***LINC00472* mitigates the influence of *miR-1275* on NSCLC malignant phenotypes**

To demonstrate that *LINC00472* could regulate the biological function of cells by binding to *miR-1275*, we carried out rescue experiments in NCI-H358 and NCI-H1299 cells. According to the results of the CCK-8 assay, proliferative potential of cells was significantly increased upon *miR-1275* overexpression, while it returned to normal level when *LINC00472* and *miR-1275* were overexpressed at the same time (NCI-H1299, oe-NC+miR-mimic compared to oe-NC+miR-NC,  $p < 0.050$ ; oe-*LINC00472*+miR-mimic compared to oe-NC+miR-mimic,  $p < 0.010$ ; NCI-H358, oe-NC+miR-mimic compared to oe-NC+miR-NC,  $p < 0.010$ ; oe-*LINC00472*+miR-mimic compared to oe-NC+miR-mimic,  $p < 0.010$ ; M–W) (Fig. 4A). Forced overexpression of *miR-1275* significantly enhanced cell migratory and invasive properties, while simultaneous overexpression of *LINC00472* and *miR-1275* significantly decreased these traits (migration: NCI-H1299, oe-NC+miR-mimic compared to oe-NC+miR-NC,  $p < 0.001$ ; oe-*LINC00472*+miR-mimic compared to oe-NC+miR-mimic,  $p < 0.001$ ; NCI-H358, oe-NC+miR-mimic compared to oe-NC+miR-NC,  $p < 0.001$ ; oe-*LINC00472*+miR-mimic compared to oe-NC+miR-mimic,  $p < 0.001$ ; invasion: NCI-H1299, oe-NC+miR-mimic compared to oe-NC+miR-NC,  $p < 0.010$ ; oe-*LINC00472*+miR-mimic compared to oe-NC+miR-mimic,  $p < 0.010$ ; NCI-H358, oe-NC+miR-mimic compared to oe-NC+miR-NC,  $p < 0.050$ , oe-*LINC00472*+miR-mimic compared to oe-NC+miR-mimic,  $p > 0.050$ ; M–W) (Fig. 4B). The apoptosis assay showed that the concurrent overexpression of both *LINC00472* and *miR-1275* could reverse the repressive effect of *miR-1275* on apoptosis rate (NCI-H1299, oe-NC+miR-mimic compared to oe-NC+miR-NC,  $p < 0.010$ ; oe-*LINC00472*+miR-mimic

compared to oe-NC+miR-mimic,  $p < 0.001$ ; NCI-H358, oe-NC+miR-mimic compared to oe-NC+miR-NC,  $p < 0.001$ ; oe-*LINC00472*+miR-mimic compared to oe-NC+miR-mimic,  $p < 0.001$ ; M–W) (Fig. 4C). Therefore, *LINC00472* could reverse the influence of *miR-1275* on NSCLC malignant cell phenotype progression.

### *LINC00472* promotes *HOXA2* expression level by restraining *miR-1275*

Targeted genes downstream of *miR-1275* were predicted using miRSearch, TargetScan and mirDIP databases, and overlapped with differentially downregulated genes screened in the GSE44077 chip (Fig. 5A). The *HOXA2* was obtained, and its expression level in GSE44077 was noticeably downregulated (Fig. 5B,  $p < 0.001$ , M–W). Our bioinformatics approach showed that *miR-1275* and *HOXA2* had targeted binding sites (Fig. 5C), and the overexpression of *miR-1275* repressed luciferase activity of *HOXA2*-WT (293T,  $p < 0.001$ , M–W) but did not affect the luciferase activity of *HOXA2*-MUT (293T,  $p > 0.05$ , M–W) (Fig. 5D), indicating that *miR-1275* could target *HOXA2*. Concurrently, the experimental RIP results demonstrated a binding relationship between *HOXA2* and *miR-1275* (AGO2: NCI-H1299,  $p < 0.001$ ; NCI-H358,  $p < 0.001$ ; M–W) (Fig. 5E,F). The above results indicate that *LINC00472* competitively bound to *miR-1275* with *HOXA2*. Using qPCR assay, we denoted that when *LINC00472* was overexpressed, the mRNA level of *miR-1275* was significantly downregulated, while the *HOXA2* level was markedly increased. In addition to *LINC00472* overexpression, simultaneous upregulation of *miR-1275* or silencing of *HOXA2* partially rescued the impact of *LINC00472* overexpression on *HOXA2* mRNA expression level (details of statistical analysis are presented in Table 4). It is commonly known that matrix metalloproteinase (MMP) and epithelial–mesenchymal transition (EMT)-related proteins are vital biomarkers associated with tumor metastasis.<sup>36–39</sup> We used western blot analysis to investigate protein levels of EMT-related proteins in order to ascertain whether the *LINC00472*/*miR-1275*/*HOXA2* axis is related to EMT processes and apoptosis in NSCLC. After overexpressing

*LINC00472*, the *E-cadherin* level was notably upregulated, but levels of *N-cadherin*, *MMP2* and *MMP9* were significantly decreased. Meanwhile, we explored protein levels of the apoptosis-related *Bax* and *Bcl-2*, and found that the overexpression of *LINC00472* enhanced pro-apoptotic *Bax* protein level but reduced anti-apoptotic protein *Bcl-2* level. Moreover, the overexpression of *miR-1275* or silencing of *HOXA2* partly rescued or even reversed the expression of the above proteins (Fig. 5H). These results highlight that *LINC00472* could promote *HOXA2* level and affect the expression of EMT, metastasis and apoptosis-related proteins by inhibiting *miR-1275*.

### *LINC00472*/*miR-1275*/*HOXA2* axis regulates NSCLC cell phenotype progression

To verify whether *LINC00472* exerted its anti-cancer effect by targeting *miR-1275* to regulate *HOXA2*, we conducted rescue experiments in NCI-H358 and NCI-H1299 cell lines. The overexpression of *LINC00472* repressed cell proliferation, migration and invasion, and promoted apoptosis, while further forced *miR-1275* expression offset the abovementioned suppressive effects (details of statistical analysis are presented in Table 5) (Fig. 6A–C). Interestingly, simultaneous overexpression of *LINC00472* and silencing of *HOXA2* also largely rescued the inhibition of *LINC00472* on malignant phenotype found in NSCLC cells (Fig. 6A–C). The above results show that the overexpression of *LINC00472* regulated *HOXA2* by targeting *miR-1275* to inhibit the proliferation, migration and invasion of NSCLC cells and promote apoptosis. These findings, combined with previous studies, demonstrate that *LINC00472* plays an essential role in regulating NSCLC cells by competitively sponging *miR-1275* with *HOXA2*.

## Discussion

Over the past 2 decades, NSCLC treatment has undergone tremendous changes. A deeper understanding of the mechanism of cancer pathogenesis has made early

**Table 4.** Statistical analysis of the expression levels of *LINC00472*, *miR-1275* and *HOXA2* in NCI-H1299 and NCI-H358 cells of each treatment group (Mann–Whitney U test; cf. Fig. 5G)

Cell lines	Group	oe- <i>LINC00472</i> compared to NC	oe- <i>LINC00472</i> + <i>miR</i> -mimic compared to oe- <i>LINC00472</i>	oe- <i>LINC00472</i> +si- <i>HOXA2</i> compared to oe- <i>LINC00472</i>
NCI-H1299	<i>LINC00472</i>	$p < 0.001$	$p > 0.050$	$p > 0.050$
	<i>miR-1275</i>	$p < 0.001$	$p < 0.001$	$p > 0.050$
	<i>HOXA2</i>	$p < 0.001$	$p < 0.001$	$p < 0.001$
NCI-H358	<i>LINC00472</i>	$p < 0.001$	$p > 0.050$	$p > 0.050$
	<i>miR-1275</i>	$p < 0.001$	$p < 0.001$	$p < 0.010$
	<i>HOXA2</i>	$p < 0.001$	$p < 0.050$	$p < 0.001$

NC – negative control.



**Table 5.** Statistical analysis of NCI-H1299 and NCI-H358 cell viability, migration, invasion, and apoptosis rate in each treatment group (Mann–Whitney U test; cf. Fig. 6A–C)

Analysis project	Group	oe-LINC00472 compared to NC	oe-LINC00472+miR-mimic compared to oe-LINC00472	oe-LINC00472+si-HOXA2 compared to oe-LINC00472
Cell viability	NCI-H1299	p < 0.010	p < 0.010	p < 0.010
	NCI-H358	p < 0.010	p < 0.010	p < 0.010
Migration	NCI-H1299	p < 0.001	p < 0.001	p < 0.001
	NCI-H358	p < 0.001	p < 0.001	p < 0.001
Invasion	NCI-H1299	p < 0.001	p < 0.001	p < 0.001
	NCI-H358	p < 0.001	p < 0.001	p < 0.001
Apoptosis rate	NCI-H1299	p < 0.001	p < 0.001	p < 0.001
	NCI-H358	p < 0.001	p < 0.001	p < 0.001

NC – negative control.

diagnosis and the development of new targeted therapies possible.<sup>40</sup> Precision medicine is the trend of the times, so it is urgent to uncover novel NSCLC biomarkers. Mounting evidence shows that lncRNAs are involved in cancer growth, differentiation, metastasis, and apoptosis.<sup>8,41</sup> We investigated the role of *LINC00472* in the progression of NSCLC and explored its regulatory mechanism.

Herein, we demonstrated that *LINC00472* and *HOXA2* expression was reduced, and *miR-1275* level was elevated in NSCLC tissues and cells. According to previous studies, *LINC-PINT*<sup>42</sup> and *FENDRR*<sup>43</sup> also have reduced expression in NSCLC similar to *LINC00472*, and act as antitumor lncRNAs, able to inhibit the progression of NSCLC. However, other lncRNAs such as *LINC01561*,<sup>44</sup> *HOTAIR*<sup>45</sup> and *H19*<sup>46</sup> are overexpressed in NSCLC and promote its progression. Lung cancer progression is closely related to changes in *HOX* gene expression, and the *HOXA* family of genes is usually downregulated in primary NSCLC.<sup>47</sup> For example, *HOXA9* is directly downregulated by *miR-196b*, and regulates NSCLC invasion potential by regulating *nuclear factor-kappa B (NF-κB)* activity.<sup>48</sup> The *HOXC* and *HOXD* family genes (such as *HOXC4*, *HOXC8*, *HOXC9*, *HOXC13*, *HOXD8*, and *HOXD10*) are highly expressed in LC<sup>47,49</sup> and are pivotal in promoting cancer. Following the previous studies on *HOXA* family genes, we found that *HOXA2* was downregulated in NSCLC and can act as a tumor repressor of cell malignant progression. Deng et al. disclosed that *LINC00472* represses EMT in lung adenocarcinoma, but the overexpression of *YBX1* restores the EMT phenotype.<sup>50</sup> Our results showed that *LINC00472* constrained EMT, but further overexpression of *miR-1275* or knockdown of *HOXA2* restored EMT, in agreement with the findings of the previous studies.

To further explore the regulatory role of *LINC00472* in NSCLC, we conducted a bioinformatics analysis on *LINC00472* and found the downstream gene *miR-1275*. One study has found that *miR-1275* is upregulated in lung adenocarcinoma, which can play a tumorigenic role by co-activating the *Wnt/β-catenin* and Notch signaling pathways in lung adenocarcinoma.<sup>51</sup> Another study

shows that lncRNA *FAM225A* can promote the occurrence and metastasis of nasopharyngeal carcinoma by targeting *miR-590-3p/miR-1275* and upregulating *ITGB3*.<sup>24</sup> Our study demonstrated that *miR-1275* was highly expressed in NSCLC. The *LINC00472* could regulate the proliferation, migration and invasion of NSCLC cells by targeting *miR-1275*, which is consistent with and builds upon previous research. Our data enrich the known regulatory network of *miR-1275* in NSCLC.

Furthermore, we found that *LINC00472* could combine with *miR-1275*, while *miR-1275* targeted *HOXA2* directly. The overexpression of *LINC00472* constrained *miR-1275* expression and increased *HOXA2* level, while the overexpression of *miR-1275* restrained *HOXA2* levels. In a study regarding the lncRNA–miRNA–mRNA signaling axis, Zhang et al. found that a low expression of *LINC00472* in osteosarcoma can control the expression of *FOXO1* by targeting *miR-300*, to regulate the occurrence of osteosarcoma.<sup>52</sup> Ye et al. displayed the stimulatory effect of *LINC00472* on apoptosis in CRC cells.<sup>9</sup> We elucidated that the overexpression of *LINC00472* facilitated apoptosis of NSCLC cancer cells, but the upregulation of *miR-1275* or silencing of *HOXA2* repressed this occurrence. To the best of our knowledge, this study is the first investigation regarding the *LINC00472/miR-1275* axis in NSCLC. The *HOXA2* is targeted by several miRNAs in a variety of cell types. For example, *miR-135* in adipose tissue-derived stem cells targets *HOXA2* to promote bone and skeleton regeneration,<sup>53</sup> and in vascular smooth muscle cells (VSMCs), *miR-3960* targets *HOXA2* to promote osteogenic trans-differentiation.<sup>54</sup> The current study is our first investigation on the targeted relationship between *miR-1275* and *HOXA2*.

Furthermore, we found that *LINC00472* could restrain NSCLC malignant cell phenotype, while forced expression of *miR-1275* or silencing of *HOXA2* partially rescued or even reversed the impact of *LINC00472* upregulation alone on NSCLC cell biological behaviors. According to the report by Zhang et al., *LINC-PINT* displays reduced expression in NSCLC. The *LINC-PINT*, as a sponge

of *miR-543*, increases *PTEN* level, thereby inhibiting NSCLC growth and migration, blocking cells in the G1 phase and promoting apoptosis.<sup>42</sup> After a critical review of the above studies, we believe that *LINC00472* also functions as a sponge of *miR-1275* to affect *HOXA2* levels, thus inhibiting the progression of NSCLC. The lncRNA *HOTAIR* is an important indicator of NSCLC diagnosis and treatment, and it can facilitate the malignant procession of LC cells.<sup>55</sup> Our study also provides possible molecular markers for NSCLC diagnosis and therapy. Moreover, *miR-1275* can facilitate the proliferation, invasion and migration of squamous cell head and neck carcinoma by increasing *IGF-1R* and *CCR7*.<sup>56</sup> Conversely, silencing *miR-1275* can significantly restrain the growth of gliomas by increasing the *Claudin11* protein level.<sup>57</sup> Furthermore, *miR-1275* can also target *ELK1* to suppress the differentiation of human visceral preadipocytes and inhibit obesity.<sup>58</sup> The methylation level of *miR-1275* is closely related to the pathogenesis of NSCLC, and *HOXA2* is a gene that is specifically methylated in NSCLC tumors.<sup>59</sup> Based on previous research results and the results of this study, we reasonably speculated that the *LINC00472/miR-1275/HOXA2* axis may be a candidate therapeutic target in NSCLC.

## Limitations

The sample size of this study was limited, and future research would benefit from a larger, more diverse study population.

## Conclusions

This study shows that the overexpression of *LINC00472* can enhance *HOXA2* level via the repression of *miR-1275* level, thus regulating proliferation, migration, invasion, apoptosis, and EMT progression of NSCLC cells. Our research provided evidence for the connection between *LINC00472*, *miR-1275* and *HOXA2*, but also offered a novel path for NSCLC therapy.

## Supplementary data

The supplementary materials are available at <https://doi.org/10.5281/zenodo.8053329>. The package contains the following files:

Supplementary Materials. Analysis of normal distribution of genes.

## ORCID iDs

Meichen Jiang  <https://orcid.org/0009-0007-7326-9480>  
 Xiangli Ye  <https://orcid.org/0009-0001-5596-5120>  
 Dongliang Shi  <https://orcid.org/0009-0003-1263-4529>  
 Qili Lin  <https://orcid.org/0009-0009-8998-3202>  
 Feijian Huang  <https://orcid.org/0009-0000-4904-677X>  
 Yong Li  <https://orcid.org/0000-0002-5842-3722>

## References

1. Siegel RL, Miller KD, Jemal A. Cancer statistics, 2019. *CA Cancer J Clin*. 2019;69(1):7–34. doi:10.3322/caac.21551
2. Rabe KF. Precision diagnosis and treatment for advanced non-small-cell lung cancer. *N Engl J Med*. 2017;377(9):849–861. doi:10.1056/NEJMra1703413
3. Travis WD, Brambilla E, Burke AP, Marx A, Nicholson AG. Introduction to The 2015 World Health Organization Classification of Tumors of the Lung, Pleura, Thymus, and Heart. *J Thorac Oncol*. 2015;10(9):1240–1242. doi:10.1097/JTO.0000000000000663
4. Osmani L, Askin F, Gabrielson E, Li QK. Current WHO guidelines and the critical role of immunohistochemical markers in the subclassification of non-small cell lung carcinoma (NSCLC): Moving from targeted therapy to immunotherapy. *Semin Cancer Biol*. 2018;52(Pt 1):103–109. doi:10.1016/j.semcancer.2017.11.019
5. Travis WD, Brambilla E, Nicholson AG, et al. The 2015 World Health Organization Classification of Lung Tumors: Impact of genetic, clinical and radiologic advances since the 2004 classification. *J Thorac Oncol*. 2015;10(9):1243–1260. doi:10.1097/JTO.0000000000000630
6. Hirsch FR, Scagliotti GV, Mulshine JL, et al. Lung cancer: Current therapies and new targeted treatments. *Lancet*. 2017;389(10066):299–311. doi:10.1016/S0140-6736(16)30958-8
7. Fang Y, Fullwood MJ. Roles, functions, and mechanisms of long non-coding RNAs in cancer. *Genomics Proteomics Bioinformatics*. 2016;14(1):42–54. doi:10.1016/j.gpb.2015.09.006
8. Bhan A, Soleimani M, Mandal SS. Long noncoding RNA and cancer: A new paradigm. *Cancer Res*. 2017;77(15):3965–3981. doi:10.1158/0008-5472.CAN-16-2634
9. Ye Y, Yang S, Han Y, et al. Linc00472 suppresses proliferation and promotes apoptosis through elevating PDCD4 expression by sponging miR-196a in colorectal cancer. *Aging (Albany NY)*. 2018;10(6):1523–1533. doi:10.18632/aging.101488
10. Sanchez Calle A, Kawamura Y, Yamamoto Y, Takeshita F, Ochiya T. Emerging roles of long non-coding RNA in cancer. *Cancer Sci*. 2018;109(7):2093–2100. doi:10.1111/cas.13642
11. Shen Y, Wang Z, Loo LW, et al. LINC00472 expression is regulated by promoter methylation and associated with disease-free survival in patients with grade 2 breast cancer. *Breast Cancer Res Treat*. 2015;154(3):473–482. doi:10.1007/s10549-015-3632-8
12. Wang Z, Katsaros D, Biglia N, et al. ERα upregulates the expression of long non-coding RNA LINC00472 which suppresses the phosphorylation of NF-κB in breast cancer. *Breast Cancer Res Treat*. 2019;175(2):353–368. doi:10.1007/s10549-018-05108-5
13. Shen Y, Katsaros D, Loo LWM, et al. Prognostic and predictive values of long non-coding RNA LINC00472 in breast cancer. *Oncotarget*. 2015;6(11):8579–8592. doi:10.18632/oncotarget.3287
14. Fu Y, Biglia N, Wang Z, et al. Long non-coding RNAs, ASAP1-IT1, FAM215A, and LINC00472, in epithelial ovarian cancer. *Gynecol Oncol*. 2016;143(3):642–649. doi:10.1016/j.ygyno.2016.09.021
15. Chen C, Zheng Q, Kang W, Yu C. Long non-coding RNA LINC00472 suppresses hepatocellular carcinoma cell proliferation, migration and invasion through miR-93-5p/PDCD4 pathway. *Clin Res Hepatol Gastroenterol*. 2019;43(4):436–445. doi:10.1016/j.clinre.2018.11.008
16. Chen Y, Pan Y, Ji Y, Sheng L, Du X. Network analysis of differentially expressed smoking-associated mRNAs, lncRNAs and miRNAs reveals key regulators in smoking-associated lung cancer. *Exp Ther Med*. 2018;16(6):4991–5002. doi:10.3892/etm.2018.6891
17. Zhu TG, Xiao X, Wei Q, Yue M, Zhang LX. Revealing potential long non-coding RNA biomarkers in lung adenocarcinoma using long non-coding RNA-mediated competitive endogenous RNA network. *Braz J Med Biol Res*. 2017;50(9):e6297. doi:10.1590/1414-431x20176297
18. Sui J, Li YH, Zhang YQ, et al. Integrated analysis of long non-coding RNA-associated ceRNA network reveals potential lncRNA biomarkers in human lung adenocarcinoma. *Int J Oncol*. 2016;49(5):2023–2036. doi:10.3892/ijo.2016.3716
19. Liu J, Song S, Lin S, et al. Circ-SERPINE2 promotes the development of gastric carcinoma by sponging miR-375 and modulating YWHAZ. *Cell Prolif*. 2019;52(4):e12648. doi:10.1111/cpr.12648
20. Bica-Pop C, Cojocneanu-Petric R, Magdo L, Raduly L, Gulei D, Berindan-Neagoe I. Overview upon miR-21 in lung cancer: Focus on NSCLC. *Cell Mol Life Sci*. 2018;75(19):3539–3551. doi:10.1007/s00018-018-2877-x

21. Liu M, Zhang Y, Zhang J, et al. MicroRNA-1253 suppresses cell proliferation and invasion of non-small-cell lung carcinoma by targeting WNT5A. *Cell Death Dis.* 2018;9(2):189. doi:10.1038/s41419-017-0218-x
22. Gao P, Wang H, Yu J, et al. miR-3607-3p suppresses non-small cell lung cancer (NSCLC) by targeting TGFBR1 and CCNE2. *PLoS Genet.* 2018;14(12):e1007790. doi:10.1371/journal.pgen.1007790
23. Xie H, Huang H, Huang W, Xie Z, Yang Y, Wang F. LncRNA miR143HG suppresses bladder cancer development through inactivating Wnt/ $\beta$ -catenin pathway by modulating miR-1275/AXIN2 axis. *J Cell Physiol.* 2019;234(7):11156–11164. doi:10.1002/jcp.27764
24. Zheng ZQ, Li ZX, Zhou GQ, et al. Long noncoding RNA FAM225A promotes nasopharyngeal carcinoma tumorigenesis and metastasis by acting as ceRNA to sponge miR-590-3p/miR-1275 and upregulate ITGB3. *Cancer Res.* 2019;79(18):4612–4626. doi:10.1158/0008-5472.CAN-19-0799
25. Xie C, Wu Y, Fei Z, Fang Y, Xiao S, Su H. MicroRNA-1275 induces radio-sensitization in oesophageal cancer by regulating epithelial-to-mesenchymal transition via Wnt/ $\beta$ -catenin pathway. *J Cell Mol Med.* 2020;24(1):747–759. doi:10.1111/jcmm.14784
26. Feng J, Li J, Qie P, Li Z, Xu Y, Tian Z. Long non-coding RNA (lncRNA) PGMSP4-AS1 inhibits lung cancer progression by up-regulating leucine zipper tumor suppressor (LZTS3) through sponging microRNA miR-1275. *Bioengineered.* 2021;12(1):196–207. doi:10.1080/21655979.2020.1860492
27. Li L, Zhang X, Liu Q, et al. Emerging role of HOX genes and their related long noncoding RNAs in lung cancer. *Crit Rev Oncol Hematol.* 2019;139:1–6. doi:10.1016/j.critrevonc.2019.04.019
28. Zhang B, Li N, Zhang H. Knockdown of homeobox B5 (HOXB5) inhibits cell proliferation, migration, and invasion in non-small cell lung cancer cells through inactivation of the Wnt/ $\beta$ -Catenin pathway. *Oncol Res.* 2018;26(1):37–44. doi:10.3727/096504017X14900530835262
29. Li D, Bai Y, Feng Z, et al. Study of promoter methylation patterns of HOXA2, HOXA5, and HOXA6 and its clinicopathological characteristics in colorectal cancer. *Front Oncol.* 2019;9:394. doi:10.3389/fonc.2019.00394
30. Li HP, Peng CC, Chung IC, et al. Aberrantly hypermethylated homeobox A2 derepresses metalloproteinase-9 through TBP and promotes invasion in nasopharyngeal carcinoma. *Oncotarget.* 2013;4(11):2154–2165. doi:10.18632/oncotarget.1367
31. Tapia-Carrillo D, Tovar H, Velazquez-Caldelas TE, Hernandez-Lemus E. Master regulators of signaling pathways: An application to the analysis of gene regulation in breast cancer. *Front Genet.* 2019;10:1180. doi:10.3389/fgene.2019.01180
32. Liu Z, Shen F, Wang H, et al. Abnormally high expression of HOXA2 as an independent factor for poor prognosis in glioma patients. *Cell Cycle.* 2020;19(13):1632–1640. doi:10.1080/15384101.2020.1762038
33. Hata A, Nakajima T, Matsusaka K, et al. A low DNA methylation epigenotype in lung squamous cell carcinoma and its association with idiopathic pulmonary fibrosis and poorer prognosis. *Int J Cancer.* 2020;146(2):388–399. doi:10.1002/ijc.32532
34. Ritchie ME, Phipson B, Wu D, et al. limma powers differential expression analyses for RNA-sequencing and microarray studies. *Nucleic Acids Res.* 2015;43(7):e47. doi:10.1093/nar/gkv007
35. Venkatesh B, Finfer S, Cohen J, et al. Adjunctive glucocorticoid therapy in patients with septic shock. *N Engl J Med.* 2018;378(9):797–808. doi:10.1056/NEJMoa1705835
36. Wang W, Li D, Xiang L, et al. TIMP-2 inhibits metastasis and predicts prognosis of colorectal cancer via regulating MMP-9. *Cell Adh Migr.* 2019;13(1):272–283. doi:10.1080/19336918.2019.1639303
37. Zhang S, Yang Y, Huang S, et al. SIRT1 inhibits gastric cancer proliferation and metastasis via STAT3/MMP-13 signaling. *J Cell Physiol.* 2019;234(9):15395–15406. doi:10.1002/jcp.28186
38. Tian S, Peng P, Li J, et al. SERPINH1 regulates EMT and gastric cancer metastasis via the Wnt/ $\beta$ -catenin signaling pathway. *Aging (Albany NY).* 2020;12(4):3574–3593. doi:10.18632/aging.102831
39. Zhang H, Wang J, Yin Y, Meng Q, Lyu Y. The role of EMT-related lncRNA in the process of triple-negative breast cancer metastasis. *Biosci Rep.* 2021;41(2):BSR20203121. doi:10.1042/BSR20203121
40. Herbst RS, Morgensztern D, Boshoff C. The biology and management of non-small cell lung cancer. *Nature.* 2018;553(7689):446–454. doi:10.1038/nature25183
41. Fatica A, Bozzoni I. Long non-coding RNAs: New players in cell differentiation and development. *Nat Rev Genet.* 2014;15(1):7–21. doi:10.1038/nrg3606
42. Wang S, Jiang W, Zhang X, et al. LINC-PINT alleviates lung cancer progression via sponging miR-543 and inducing PTEN. *Cancer Med.* 2020;9(6):1999–2009. doi:10.1002/cam4.2822
43. Zhang G, Wang Q, Zhang X, Ding Z, Liu R. LncRNA FENDRR suppresses the progression of NSCLC via regulating miR-761/TIMP2 axis. *Biomed Pharmacother.* 2019;118:109309. doi:10.1016/j.biopha.2019.109309
44. Gao W, Qi C, Feng M, Yang P, Liu L, Sun S. SOX2-induced upregulation of lncRNA LINC01561 promotes non-small-cell lung carcinoma progression by sponging miR-760 to modulate SHCBP1 expression. *J Cell Physiol.* 2020;235(10):6684–6696. doi:10.1002/jcp.29564
45. Jiang C, Yang Y, Yang Y, et al. Long noncoding RNA (lncRNA) HOTAIR affects tumorigenesis and metastasis of non-small cell lung cancer by upregulating miR-613. *Oncol Res.* 2018;26(5):725–734. doi:10.3727/096504017X15119467381615
46. Huang Z, Lei W, Hu H, Zhang H, Zhu Y. H19 promotes non-small-cell lung cancer (NSCLC) development through STAT3 signaling via sponging miR-17. *J Cell Physiol.* 2018;233(10):6768–6776. doi:10.1002/jcp.26530
47. Bhatlekar S, Fields JZ, Boman BM. HOX genes and their role in the development of human cancers. *J Mol Med (Berl).* 2014;92(8):811–823. doi:10.1007/s00109-014-1181-y
48. Yu SL, Lee DC, Sohn HA, et al. Homeobox A9 directly targeted by miR-196b regulates aggressiveness through nuclear factor-kappa B activity in non-small cell lung cancer cells. *Mol Carcinog.* 2016;55(12):1915–1926. doi:10.1002/mc.22439
49. Omatu T. Overexpression of human homeobox gene in lung cancer A549 cells results in enhanced motile and invasive properties [in Japanese]. *Hokkaido Igaku Zasshi.* 1999;74(5):367–376. PMID:10495851.
50. Deng X, Xiong W, Jiang X, et al. LncRNA LINC00472 regulates cell stiffness and inhibits the migration and invasion of lung adenocarcinoma by binding to YBX1. *Cell Death Dis.* 2020;11(11):945. doi:10.1038/s41419-020-03147-9
51. Jiang N, Zou C, Zhu Y, et al. HIF-1 $\alpha$ -regulated miR-1275 maintains stem cell-like phenotypes and promotes the progression of LUAD by simultaneously activating Wnt/ $\beta$ -catenin and Notch signaling. *Theranostics.* 2020;10(6):2553–2570. doi:10.7150/thno.41120
52. Zhang J, Zhang J, Zhang D, Ni W, Xiao H, Zhao B. Down-regulation of LINC00472 promotes osteosarcoma tumorigenesis by reducing FOXO1 expressions via miR-300. *Cancer Cell Int.* 2020;20:100. doi:10.1186/s12935-020-01170-6
53. Xie Q, Wang Z, Zhou H, et al. The role of miR-135-modified adipose-derived mesenchymal stem cells in bone regeneration. *Biomaterials.* 2016;75:279–294. doi:10.1016/j.biomaterials.2015.10.042
54. Xia ZY, Hu Y, Xie PL, et al. Runx2/miR-3960/miR-2861 positive feedback loop is responsible for osteogenic transdifferentiation of vascular smooth muscle cells. *Biomed Res Int.* 2015;2015:624037. doi:10.1155/2015/624037
55. Loewen G, Jayawickramarajah J, Zhuo Y, Shan B. Functions of lncRNA HOTAIR in lung cancer. *J Hematol Oncol.* 2014;7:90. doi:10.1186/s13045-014-0090-4
56. Liu MD, Wu H, Wang S, et al. MiR-1275 promotes cell migration, invasion and proliferation in squamous cell carcinoma of head and neck via up-regulating IGF-1R and CCR7. *Gene.* 2018;646:1–7. doi:10.1016/j.gene.2017.12.049
57. Katsushima K, Shinjo K, Natsume A, et al. Contribution of microRNA-1275 to Claudin11 protein suppression via a polycomb-mediated silencing mechanism in human glioma stem-like cells. *J Biol Chem.* 2012;287(33):27396–27406. doi:10.1074/jbc.M112.359109
58. Pang L, You L, Ji C, et al. miR-1275 inhibits adipogenesis via ELK1 and its expression decreases in obese subjects. *J Mol Endocrinol.* 2016;57(1):33–43. doi:10.1530/JME-16-0007
59. Heller G, Babinsky VN, Ziegler B, et al. Genome-wide CpG island methylation analyses in non-small cell lung cancer patients. *Carcinogenesis.* 2013;34(3):513–521. doi:10.1093/carcin/bgs363